BULLETIN OF THE POLISH ACADEMY OF SCIENCES
TECHNICAL SCIENCES, Vol. 74(1), 2026, Article number: e156765
DOI: 10.24425/bpasts.2025.156765

CONTROL, INFORMATICS AND ROBOTICS

Fault detection method for DFIG based on particle swarm optimized sliding mode observer

Tingting XIE[1]*, **Hongwei ZHANG**[2], and **Chenjia NI**[3]

[1] Shanghai Industrial and Commercial Polytechnic, Shanghai 200000, China
[2] Jiangsu Hongdou Energy Technology Co., Ltd, Wuxi 214000, China
[3] Harbin Welding Institute Limited Company, Harbin 150000, China

Abstract. The traditional sliding mode observer can achieve effective fault detection by reconstructing the doubly-fed induction generators (DFIG) model and comparing it with the measurable state quantity. However, unreasonable sliding mode observer parameters will greatly reduce the accuracy of fault detection and even cause false alarms. Aiming at the difficulty of selecting sliding mode parameters, this paper proposes to combine particle swarm optimization (PSO) algorithm with sliding mode observer for fault detection of DFIG. This method can obtain extremely high observation accuracy while minimizing chattering in the observer. First, this paper designs a sliding mode observer based on the mathematical model of the DFIG. Then, the PSO algorithm is used to find the optimal sliding mode observer gain. Finally, the normal operating conditions, the voltage drop fault of the grid terminal and the rotor current sensor fault are set, and on this basis, Simulink simulation models under different fault conditions are established. After comparing the actual rotor current value and the residual error of the observed value, the fault detection is realized. It is proven by simulation that this sliding mode observer can realize fault detection well, and it can be seen that the sliding mode observer has the characteristics of fast response speed and high accuracy.

Keywords: DFIG; fault detection; PSO; sliding mode observer.

1. INTRODUCTION

Doubly-fed induction generators (DFIG) are currently the most widely used wind generators. It consists of a wound asynchronous generator with a stator winding directly connected to a fixed frequency three-phase grid and a back-to-back converter installed on the rotor winding [1]. Mainly through power electronic technology, vector control technology and microcomputer information processing technology to achieve high-performance control of DFIG, so as to obtain a stable, high-quality electrical energy. Due to the complex internal structure and harsh operating environment of DFIG, the system components are prone to electrical and mechanical failures. Once a failure occurs in the system, it will cost a lot to repair the failure. Therefore, the DFIG control system should have the ability to detect early faults online, improve the reliability of wind turbines, and reduce maintenance costs [2–4].

There are currently two common fault detection methods. One is a method that does not rely on analytical models [5, 6], such as neural network algorithms and support vector machines. The other is methods that rely on analytical models [7, 8], such as Kalman filters, state observers. [9] imported the vibration signal characteristics of wind turbines into a long short-term memory (LSTM) network for training to detect early failures of wind turbines. Since the supervisory control and data acquisition (SCADA) system of the wind turbine generator provides a wealth of sensor information, [10] developed a multiscale spatio-temporal convolutional deep belief network (MSTCDBN). By capturing the hidden spatio-temporal features in SCADA data, feature learning and classification are performed to achieve DFIG fault detection. This method can not only learn the spatial correlation information between several different variables, but also capture the temporal characteristics of each variable. In view of the limited fault data set collected during the actual operation of wind turbines, [11] proposed a data enhancement method based on Hermite interpolation, and then diagnosed wind turbine faults by designing a spherical data model. [12] proposed a dendritic cell algorithm (DCA) based on the immune system (IS) inspired mechanism. In the case of given dual sensor redundancy, both detection and sensor failure can be isolated. For the faults caused by sensor aging, [13] is characterized by the slow change of the sensor measurement noise covariance matrix. The quality information of the weighted innovation sequence is used to estimate the sensor noise covariance. In the fault detection method based on the analytical model, the estimated value is obtained by setting the fault observer. Determine whether a fault occurs according to the observation residuals, which provides an effective way for the measurement of status information. It avoids the system expenditure and hardware complexity caused by traditional measurement methods. [14] and [15] studied the stability of the rotor current when the stator voltage is affected by a nearby grid fault. A fault observer is proposed to detect the stator voltage fault and determine the appropriate switching time of the fault

---

*e-mail: xie_tingting@sicp.edu.cn

Manuscript submitted 2024-12-03, revised 2025-08-28, initially accepted for publication 2025-10-07, published in January 2026.

© 2026 The Author(s). This is an open access article under the CC BY license (http://creativecommons.org/licenses/by/4.0/)

stabilizer. In [16], a new diagnostic method based on an augmented state and disturbance observer is proposed for DFIG to handle insulated gate bipolar transistor (IGBT) faults, rotor and stator current sensor outages, and stator voltage sensor outages. Sliding mode observer can remain insensitive to external disturbances when observing nonlinear systems, and are widely used in fault diagnosis. In order to improve the reliability of the cascaded brushless doubly-fed induction generator wind energy conversion system (CBDFIG-WECS), [17] designed a sliding mode observer to detect faults based on the residual of the observation signal and the measurement signal.

But there are still some problems with sliding mode observers: Observer gain is usually obtained through experience. Unreasonable gain selection often occurs, but a larger gain may cause chattering of the observed value, and a smaller gain makes the observed value converge too slowly, or even diverge. Particle swarm optimization (PSO) is one of the most well-known swarm intelligence-based optimization techniques inspired by nature [18, 19]. Owing to its flexibility and ease of implementation, it has been widely applied in various optimization scenarios. For example, in [20], the PSO technique is employed to enhance the performance of the observation process by optimally tuning the parameters of a Luenberger observer according to a specified performance index. Motivated by this, the present paper proposes a PSO-optimized sliding mode observer (PSO-SMO) for fault detection of DFIGs, aiming to determine the optimal observer gains and thereby improve fault detection capability. The simulation proves that the method can obtain the best gain of the sliding mode observer, and has the characteristics of fast response and high observation accuracy. The rest of this paper is arranged as follows: Section 2 introduces the PSO algorithm. Section 3 introduces the design of PSO-SMO method. In Section 4, the convergence analysis of the sliding mode observer is carried out. In Section 5, we discuss the use of PSO-SMO to perform fault detection experiments on DFIG faults under three different operating conditions. The last section summarizes the paper. Figure 1 is a control structure diagram of DFIG based on stator voltage orientation [21].

2. PSO ALGORITHM PRINCIPLE

PSO is a swarm intelligence algorithm. Each particle in the algorithm represents a potential solution to the problem, and each particle obtains the corresponding fitness value according to the fitness function. The speed of a particle determines the direction and distance of the particle movement, and the speed is dynamically adjusted according to the movement experience of itself and other particles, so as to realize the optimization of the individual in the solvable space [22].

Suppose there is a population $X = (X_1, X_2, \dots X_n)$ composed of n particles in a D-dimensional search space, where the i-th particle is represented as a D-dimensional vector $X = (X_{i1}, X_{i2}, \dots X_{iD})^T$, namely the position of the ith particle in the D-dimensional search space. Calculate the fitness value corresponding to each particle position X according to the fitness function $F(X_i)$.

The velocity of the i-th particle is $V = (V_{i1}, V_{i2}, \dots V_{iD})^T$, is, and the optimal position it has found so far is called the individual extreme value $P_{\text{best}} = (P_{i1}, P_{i2}, \dots P_{iD})^T$. In each iteration process, the particle updates its own speed and position according to the individual extreme value and the global extreme value. The update formula is as follows:

$$V_{id}^{k+1} = \omega V_{id}^{k} + c_1 r_1 \left(P_{id}^{k} - X_{id}^{k}\right) + c_2 r_2 \left(P_{gd}^{k} - X_{id}^{k}\right), \tag{1}$$

$$X_{id}^{k+1} = X_{id}^{k} + V_{id}^{k+1}, \tag{2}$$

where $d = 1, 2, \dots, D, i = 1, 2, \dots, n$, ω is the inertia weight, k is the current iteration times, V_{id} is the velocity of the particle, c_1 and c_2 are acceleration factors, r_1 and r_2 are random numbers

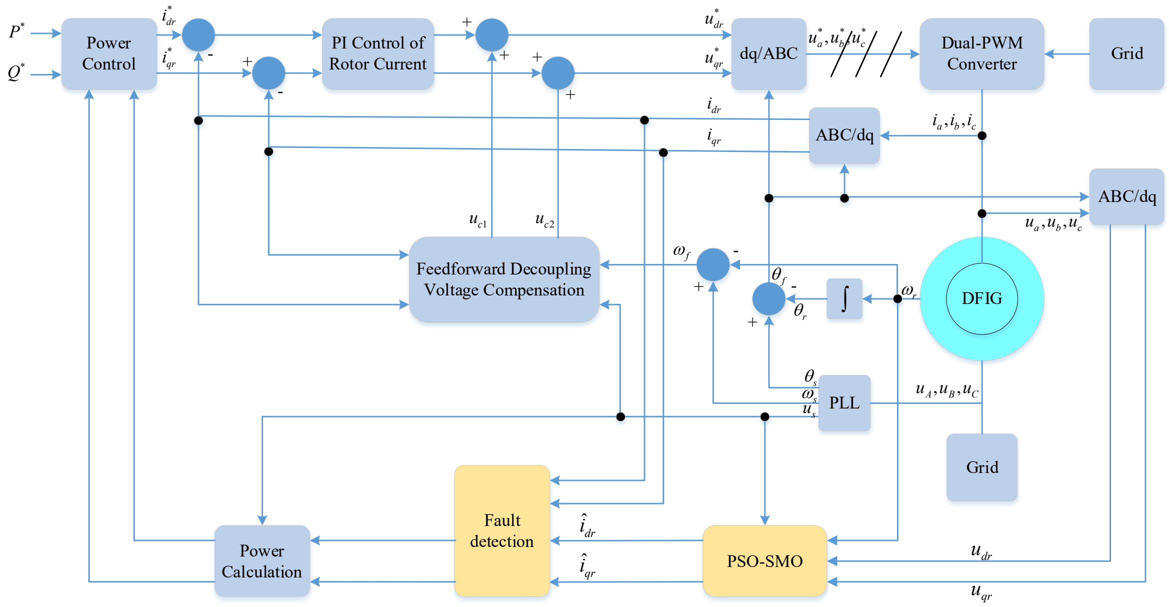

Fig. 1. DFIG control structure diagram of sliding mode observer for stator voltage orientation

distributed between $[0,1]$. In order to prevent blind search of particles, the position and velocity are limited to $[-X_{\max}, X_{\max}]$, $[-V_{\max}, V_{\max}]$ respectively.

3. OBSERVER DESIGN

3.1. Mathematical model of DFIG

The DFIG uses a wound three-phase asynchronous motor. In order to independently control the active power and reactive power of the DFIG, the stator voltage-oriented vector control method is used to transform the three-phase static coordinate system into a synchronous rotating coordinate system [23, 24]. In this paper, the rotor current is the observation object, so only the state space model of the rotor current is considered

$$\begin{cases} \dot{i_r} = Ai_r + Bu + f, \\ y = Ci_r, \end{cases} \tag{3}$$

where

$$A = \begin{bmatrix} \dfrac{-R_s L_m^2}{\sigma L_s^2 L_r} - \dfrac{R_r}{\sigma L_r} & \omega_s - \omega_r \\ \omega_r - \omega_s & \dfrac{-R_s L_m^2}{\sigma L_s^2 L_r} - \dfrac{R_r}{\sigma L_r} \end{bmatrix},$$

$$B = \begin{bmatrix} \dfrac{-L_m}{\sigma L_s L_r} & 0 & \dfrac{1}{\sigma L_r} & 0 \\ 0 & \dfrac{-L_m}{\sigma L_s L_r} & 0 & \dfrac{1}{\sigma L_r} \end{bmatrix}, \quad \begin{bmatrix} \dfrac{\omega_f - \omega_s}{\sigma L_r L_s} L_m \psi_s \\ \dfrac{R_s L_m \psi_s}{\sigma L_s^2 \psi_s} L_r \end{bmatrix}.$$

3.2. Design of sliding mode observer

According to the mathematical model of DFIG, a sliding mode observer is established. The structure is as follows:

$$\begin{cases} \dot{\hat{i_r}} = A\hat{i_r} + Bu + f + u_{eq}, \\ y = C\hat{i_r}, \end{cases} \tag{4}$$

where u_{eq} is the equivalent control item.

Let the sliding mode surface $s = \begin{bmatrix} s_d \\ s_q \end{bmatrix} = \begin{bmatrix} i_{dr} - \hat{i_{dr}} \\ i_{qr} - \hat{i_{qr}} \end{bmatrix}$, then the error equation can be obtained by subtracting (3) from (4)

$$\dot{s} = As + u_{eq}. \tag{5}$$

Let $\dot{s} = 0$, the equivalent control item can be obtained

$$u_{eq} = -As. \tag{6}$$

In order to improve the robustness of the observer and ensure that the sliding mode reachability condition is established, that is, $s\dot{s} \le 0$.

On the basis of the above observer, the switching control item u_{sm} is added, as shown in (7)

$$u_{sw} = \begin{bmatrix} k_1 s_d + \varepsilon_1 |s_d|^{0.5} \operatorname{sign}(s_d) \\ k_2 s_d + \varepsilon_2 |s_d|^{0.5} \operatorname{sign}(s_d) \end{bmatrix}. \tag{7}$$

In summary, the sliding mode observer established in this paper is

$$\begin{cases} \dot{\hat{i_r}} = A\hat{i_r} + Bu + f + v, \\ y = C\hat{i_r}, \end{cases} \tag{8}$$

where $v = u_{eq} + u_{sw}$ is the sliding mode control law, then

$$\begin{aligned} v &= \begin{bmatrix} v_1 \\ v_2 \end{bmatrix} \\ &= \begin{bmatrix} \left(\dfrac{-R_s L_m^2}{\sigma L_s^2 L_r} - \dfrac{R_r}{\sigma L_r}\right) s_d + \omega_f s_q + k_1 s_d + \varepsilon_1 |s_d|^{0.5} \operatorname{sign}(s_d) \\ -\omega_f + \left(\dfrac{-R_s L_m^2}{\sigma L_s^2 L_r} - \dfrac{R_r}{\sigma L_r}\right) s_q + k_2 s_q + \varepsilon_2 \left|s_q\right|^{0.5} \operatorname{sign}(s_q) \end{bmatrix}. \end{aligned} \tag{9}$$

When the observer satisfies the Lyapunov's stability theorem, the system state error will reach the sliding mode surface within a finite time, that is, the observer converges. Among them, the gain of a sliding mode observer k_1, k_2, ε_1, ε_2 is very important to the performance of the observer. When the gain selection of the sliding mode observer is unreasonable, it will directly affect the overall performance of the observer. When the gain selection of the sliding mode observer is unreasonable, it will directly affect the overall performance of the observer, and cause serious false alarms. In order to improve the robustness, a larger gain parameter is usually required, but this may cause chattering of the observed value. The smaller gain makes the observation value converge too slowly, and the anti-interference ability is insufficient. Therefore, this paper applies the PSO algorithm and designs the objective function needed to find the optimal gain of the sliding mode observer, so as to solve the parameter selection problem of the sliding mode observer.

Through the mathematical model of the DFIG, the PSO algorithm and the design of the sliding mode observer, the structure of the rotor current observer is shown in Fig. 2. It is divided into two parts, namely the rotor current sliding mode observer part and the PSO algorithm optimization part. The rotor current observer is built according to (8), and the PSO optimization module is built according to Section 2 in the text, where R_{th} is the preset lower limit of fitness, and $F(X_i)$ is the fitness function. In order to minimize the chattering of the sliding mode observer and obtain higher observation accuracy, the fitness function is designed as

$$\begin{aligned} F(X_i) = {} & \alpha \underbrace{\left(\int_{t_0}^{T} t\,|s_d|\,\mathrm{d}t + \int_{t_0}^{T} t\,\left|s_q\right|\,\mathrm{d}t \right)}_{1} \\ & + \beta \underbrace{\left(\int_{t_0}^{T} t\,|s_d|\,\mathrm{d}t - \int_{t_0}^{T} t\,\left|s_q\right|\,\mathrm{d}t \right)}_{2}. \end{aligned} \tag{10}$$

where $[t_0, T]$ represents the convergence interval of the sliding mode observer. The goal of the first part of (10) is to minimize

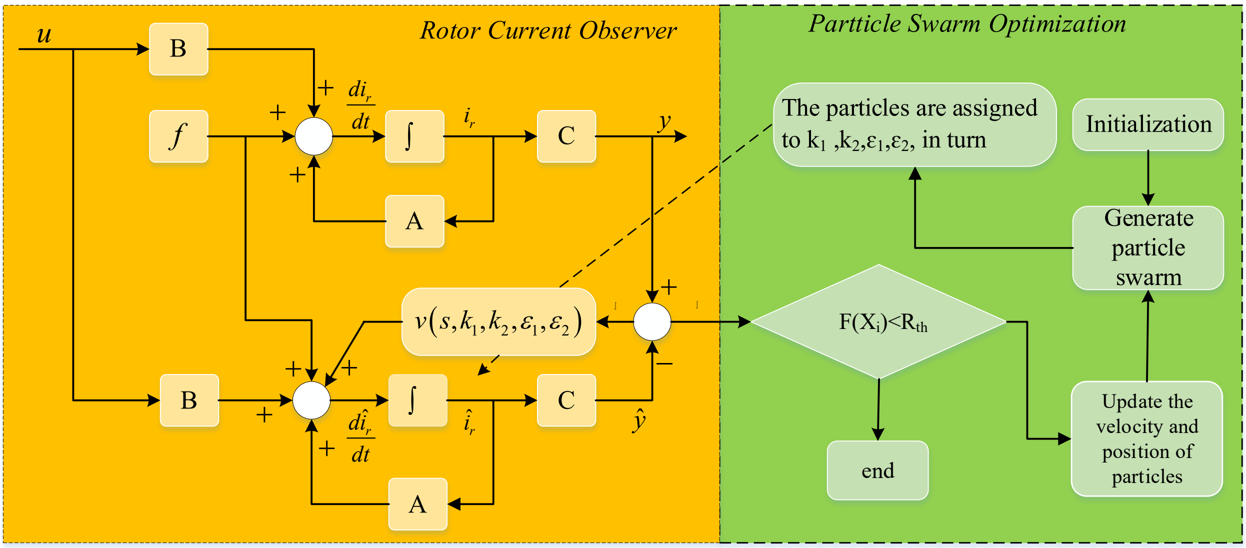

Fig. 2. PSO-SMO principle diagram

the steady-state error of the rotor currents of the d and q axes, as expressed in the first part of (10). Meanwhile, to avoid extreme cases (where the observation error of one axis current is large while the error of the other axis current is small, causing the overall fitness value to still appear minimal), an additional term related to the rotor current errors of the d-axis and q-axis is introduced, namely the second part of the equation.

$\left[t_0, T\right]$ is the convergence interval of the sliding mode observer. At the same time, in order to avoid extreme situations (the observation error of one axis current is large, while the other axis current error is small, so that the overall fitness value is still at the minimum). Therefore, an error function of the rotor current between the d-axis and the q-axis is added, which is shown in the second part of (10). α and β are the weight ratio. By adjusting the relative size, the importance of each part in (10) can be expressed separately.

The steps of the PSO-SMO algorithm:

1. Initialize the particle swarm. Including the group size n, the position X_i and velocity V_i of each particle are randomly generated, at this time $k = 1$.
2. Assign each particle to the control rate v, and calculate the fitness value $F(X_i)$ of each particle according to 10.
3. For each particle X_i, compare its fitness value $F(X_i)$ with the fitness value $F(P_{\text{best}}(i))$ of the individual extreme value $P_{\text{best}}(i)$, if $F(X_i) < F(P_{\text{best}}(i))$, replace $F(P_{\text{best}}(i))$ with $F(X_i)$.
4. For each particle X_i, compare its fitness value $F(X_i)$ with the fitness value $F(G_{\text{best}})$ of the population extremum G_{best}. If $F(X_i) < F(G_{\text{best}})$, replace $F(G_{\text{best}})$ with $F(X_i)$.
5. Update the velocity (X_i^k and position (V_i^k of particle according to (1) and (2), at this time $k = k+1$, and then return to step 2. If the termination condition is met (the maximum number of iterations or $F(X_i) < R_{th}$ is reached), the algorithm is exited and the optimal solution k_1, k_2, ε_1, ε_2 is obtained.

4. CONVERGENCE ANALYSIS

4.1. Stability analysis

Theorem 1. Define the Lyapunov function as follows:

$$V = \frac{1}{2} s^T s. \tag{11}$$

If $\dot{V} = \dot{s}^T s + s^T \dot{s} \le 0$, the observer converges progressively.

Proof.

$$\begin{aligned}
\dot{V} &= \dot{s}^T s + s^T \dot{s} \\
&= \begin{bmatrix} \dot{s}_d & \dot{s}_q \end{bmatrix} \begin{bmatrix} s_d \\ s_q \end{bmatrix} + \begin{bmatrix} s_d & s_q \end{bmatrix} \begin{bmatrix} \dot{s_d} \\ \dot{s_q} \end{bmatrix} \\
&= 2\left(\dot{s}_d s_d + \dot{s}_q s_q\right) \\
&= 2\left(-k_1 s_d^2 - \varepsilon_1 \left|s_d\right|^{3/2} - k_2 s_q^2 - \varepsilon_2 \left|s_q\right|^{3/2}\right).
\end{aligned}$$

Since k_1, k_2, ε_1 and ε_2 are positive real number, $\dot{V} \le 0$. According to the Lyapunov's stability theorem, the sliding mode observer is stable. □

4.2. Robustness

In order to enable the sliding mode observer to accurately observe the rotor current in the presence of interference, it is necessary to analyze the robustness of the sliding mode observer.

Theorem 2. Consider the rotor current model with uncertain interference $d(t)$, when $d(t) = \begin{bmatrix} d_1 \\ d_2 \end{bmatrix} \le \begin{bmatrix} M_1 \\ M_2 \end{bmatrix}$, under the action of sliding mode control law, the observer error will converge to the following region

$$|s_d| < \frac{M_1}{k_1}, \quad |s_d| < \frac{M_2}{k_2}.$$

Proof. In the case of interference, the mathematical model of the system is

$$\begin{cases} \dot{i_r} = Ai_r + Bu + f + d(t), \\ y = Ci_r \,. \end{cases} \tag{12}$$

The designed sliding mode observer is shown in (8), and subtracting (8) from (12) can be obtained

$$\begin{aligned} \dot{s} &= A\left(i_r - \hat{i}_r\right) + d(t) - A\left(i_r - \hat{i}_r\right) + \left(-ks - \varepsilon|s|^{0.5} \cdot \operatorname{sign}(s)\right) \\ &= d(t) - ks - \varepsilon|s|^{0.5} \cdot \operatorname{sign}(s). \end{aligned} \tag{13}$$

According to Lyapunov's stability theorem, when $s^T\dot{s} \le 0$, the system is still stable in the presence of interference $d(t)$.

$$\begin{aligned} s^T s &= \dot{s}_d s_d + \dot{s}_q s_q \\ &= \left(-\frac{R_r L_m^2}{\sigma L_r^2 L_t} - \frac{R_r}{\sigma L_t}\right)\left(i_{dr} - \hat{i}_{dr}\right)s_d + \omega_f\left(i_{qr} - \hat{i}_{qr}\right)s_d \\ &\quad - v_1 + s_d d_1(t) + (-\omega_f)\left(i_{dr} - \hat{i}_{dr}\right)s_q \\ &\quad + \left(-\frac{R_r L_m^2}{\sigma L_r^2 L_t} - \frac{R_r}{\sigma L_t}\right)\left(i_{qr} - \hat{i}_{qr}\right)s_q - v_2 + s_q d_2(t) \\ &= -k_1 s_d^2 - \epsilon_1 |s_d|^{\frac{3}{2}} + s_d d_1(t) - k_2 s_q^2 - \epsilon_2 \left|s_q\right|^{\frac{3}{2}} + s_q d_2(t) \\ &\le (d_1 - k_1|s_d|)|s_d| + \left(d_2 - k_2\left|s_q\right|\right)\left|s_q\right| \\ &\quad - \epsilon_1 |s_d|^{\frac{3}{2}} - \epsilon_2 \left|s_q\right|^{\frac{3}{2}} \end{aligned} \tag{14}$$

when $\begin{cases} d_1 - k_1|s_d| < 0, \\ d_2 - k_2|s_q| < 0. \end{cases}$, then $s^T\dot{s} < 0$, and the system converges. Therefore, the system status error will remain in the area:

$$\begin{cases} |s_d| < \dfrac{M_1}{k_1}, \\ |s_q| < \dfrac{M_2}{k_2}. \end{cases} \tag{15}$$

□

4.3. Convergence in finite time

Theorem 3. Under the action of the control law, the system error equation is

$$\dot{s} = -ks - \varepsilon_1|s|^{0.5}\operatorname{sign}(s). \tag{16}$$

If $k, \varepsilon > 0$, then $s, \dot{s}$ will tend to 0 within a finite time.

Proof. Multiply both ends of (16) by e^{kt} at the same time, and get

$$\frac{d\left(e^{kt} \cdot s\right)}{dt} = -\varepsilon\left|e^{kt} \cdot s\right|^{0.5} \cdot e^{\frac{kt}{2}} \cdot \operatorname{sign}(s). \tag{17}$$

(17) is simplified to

$$\frac{d\left(e^{kt} \cdot s\right)}{\left|e^{kt} \cdot s\right|^{0.5} \cdot \operatorname{sign}(s)} = -\varepsilon e^{\frac{kt}{2}}\, dt. \tag{18}$$

Integrate both sides of (18) at the same time to get

$$s(t) = \begin{cases} \operatorname{sign}(s(0)) \cdot e^{-kt}\left[|s(0)|^{0.5} + \frac{\varepsilon}{k} - \frac{\varepsilon}{k} \cdot e^{\frac{kt}{2}}\right]^2, & t_r < \dfrac{\ln\left(1 + \dfrac{\varepsilon}{k}|s(0)|^{0.5}\right)}{0.5k} \\ 0, & t_r > \dfrac{\ln\left(1 + \frac{\varepsilon}{k}|s(0)|^{0.5}\right)}{0.5k}. \end{cases} \tag{19}$$

From equation (16), it can be seen that a and b will approach 0 within a finite time t_r. □

5. SIMULATION EXPERIMENT

This paper mainly analyzes three operating conditions, which are normal operating conditions, voltage drop faults at the power grid terminal, and rotor current sensor faults. In order to verify the feasibility and correctness, this paper uses MATLAB/SIMULINK to build a vector control DFIG simulation model. According to the residual difference between the observed value of the rotor current output by the built PSO-SMO module and the actual value, the fault detection of the system is realized.

Table 1
Main parameters of DFIG system

Item	Value	Item	Value
Grid voltage (V)	220	Nominal power (VA)	3730
Grid frequency (Hz)	50	Voltage (line-line) (V)	460
DC bus voltage (V)	600	Number of pole pairs	4
Wind speed (m/s)	< 12	$R_s\,(\Omega)$	1.115
Wind turbine blade radius (m)	2	$R_r\,(\Omega)$	1.083
Gearbox transmission ratio	1:3	$L_{\sigma s}$, $L_{\sigma r}$ (mH)	5.974
		L_m	0.2037

5.1. Simulation conditions

The simulation parameters of the PSO-SMO algorithm are as follows: $n = 2$, $w = 0.2$, $c_1 = c_2 = 0.4$, $\alpha = 3$, $\beta = 1$, $t_0 = 0.15$ s, $T = 1$ s. The minimum fitness value is preset to be $R_{th} = 0$, the maximum number of iterations is $k_{\max} = 25$, and the particle search range is $[0, 20000]$. When the conditions are met(the maximum number of iterations $k_{\max} = 25$ or $F(G_{\text{best}}) < R_{th}$), the algorithm exits and the optimal gain k_1, k_2, ε_1, ε_2 of the sliding mode observer is obtained. By comparing with the traditional sliding mode observer, the effectiveness of the proposed method is proven, and it has many advantages.

5.2. Normal

In the case of no fault, set the wind speed to 6 m/s, and optimize the sliding mode observer through the PSO algorithm. In order to reduce the chattering of the observer, the optimization objective of this paper mainly considers the steady-state process of the observer. After the observer converges, the steady-state error can be regarded as a fixed value. In order to reduce the time-consuming process of parameter optimization, the steady-state error within a period of time can be selected to calculate the fitness function, that is, the integration interval of the fitness function is set to $[t_0, T]$. Figure 3 shows the changing process of the fitness value during the optimization process. When the fitness value reaches the minimum, it indicates that the gain parameter is optimal at this time. It can be seen from the figure that the fitness value gradually decreases during the iteration, and approaches the minimum value of $9.06 \cdot 10^{-3}$ after 20 iterations. Figure 4 shows the gain variation curve of the sliding mode observer. In the first iteration, k_1, k_2, ε_1, ε_2 are randomly selected. After 20 iterations, each gain curve gradually becomes stable, and finally the optimal gains are $k_1 = 11892$, $k_2 = 11739$, $\varepsilon_1 = 5189$, $\varepsilon_2 = 8567$, respectively.

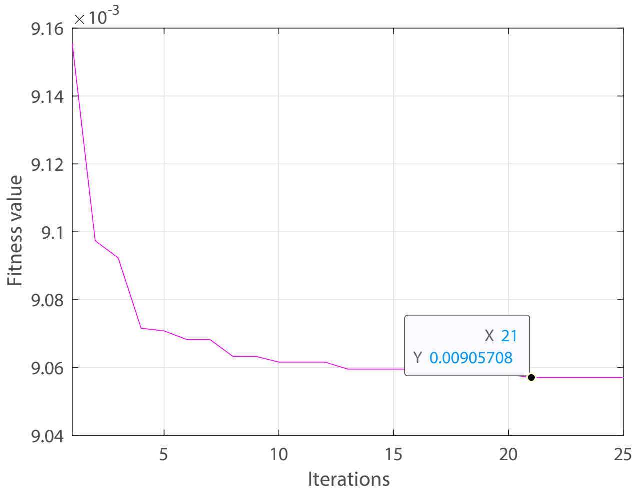

Fig. 3. Fitness curve

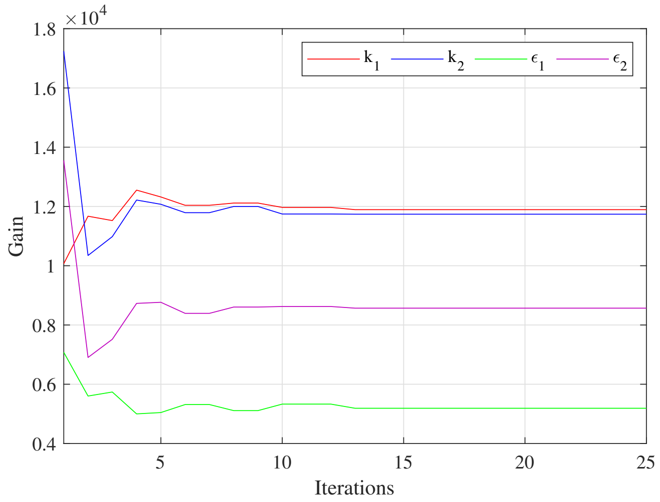

Fig. 4. Gain curve

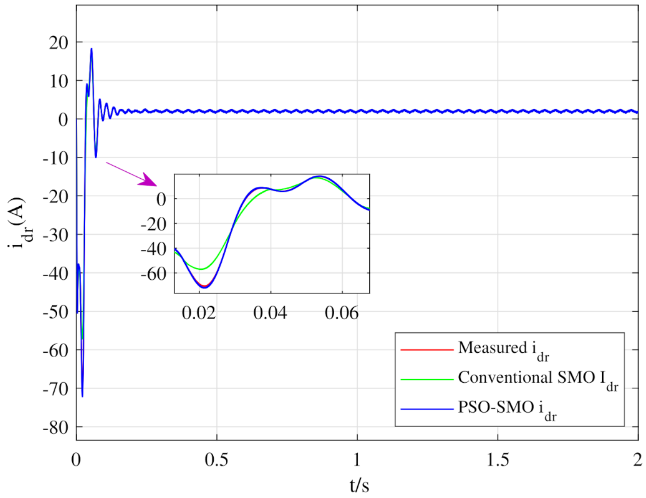

Fig. 5. Measured and observed tracking curve of rotor current d-axis

The obtained optimal parameters are imported into the sliding mode observer for fault detection experiments. Figure 5 shows the tracing curve of the measured and observed values of the rotor current d-axis. Figure 6 shows the error curve between the measured value and the observed value of the rotor current d-axis. Two kinds of sliding mode observers are used to observe the rotor current, namely the traditional sliding mode observer and PSO-SMO. It can be seen from the observation accuracy and error curve that the two sliding mode observers can track the rotor current value well, and the observation error in the steady state is about 10^{-3}. By comparing the traditional sliding mode observer with PSO-SMO, it can be found that in the process of reaching the sliding mode surface, the traditional sliding mode observer has a large error, while the PSO-SMO has a very small error. In addition, the PSO-SMO observation accuracy is higher and the response speed is faster. Figure 7 shows the tracking curve of measured and observed values of rotor current q-axis. Figure 8 shows the error curve between the measured value and the observed value of the rotor current q-axis. It has a similar change process with the d-axis current, and it can still be seen that PSO-SMO performs better than the traditional sliding mode observer.

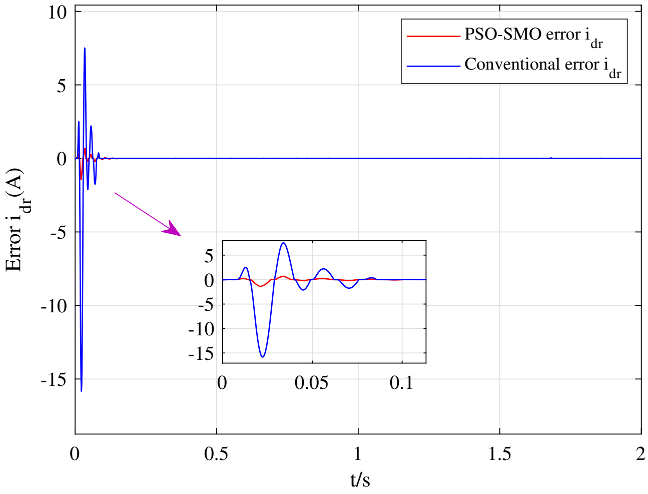

Fig. 6. Error curve between measured value and observed value of rotor current d-axis

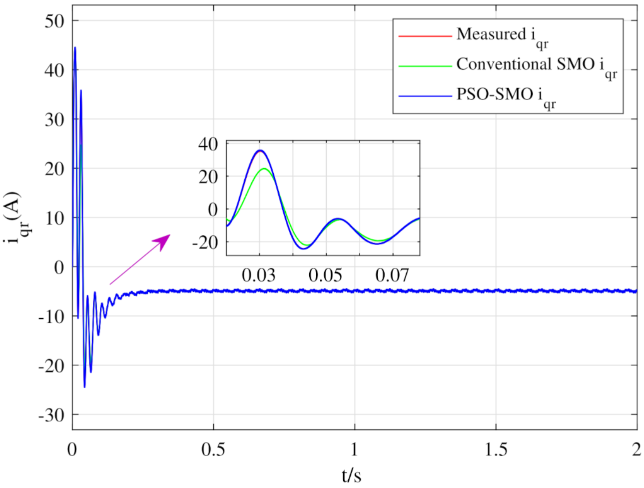

Fig. 7. Measured and observed tracking curve of rotor current q-axis

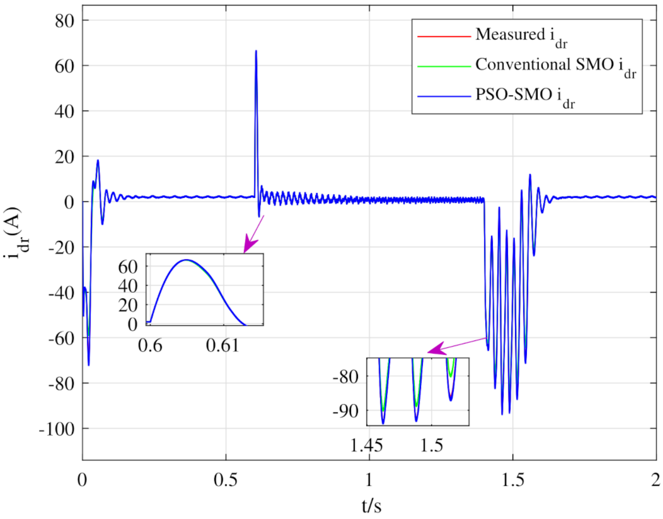

Fig. 9. Measured and observed tracking curve of rotor current d-axis

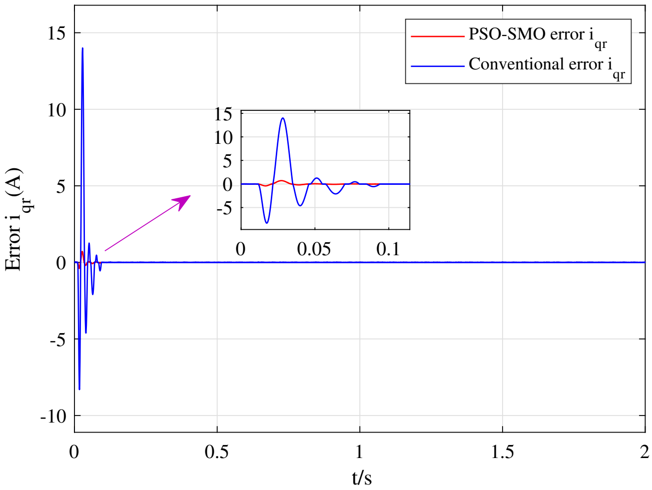

Fig. 8. Error curve between measured value and observed value of rotor current q-axis

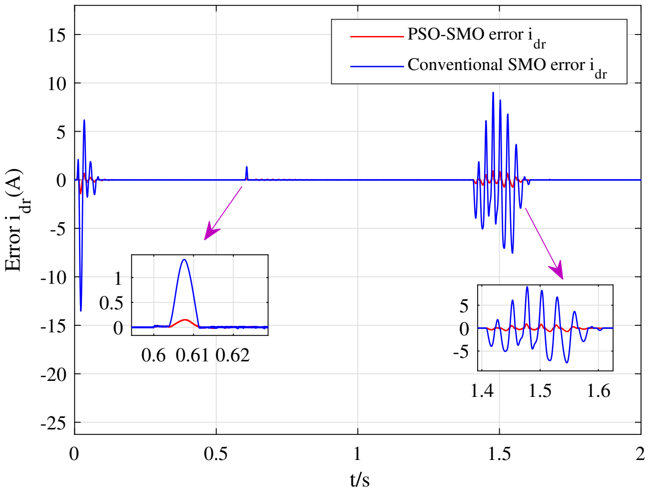

Fig. 10. Error curve between measured value and observed value of rotor current d-axis

5.3. Voltage drop failure

In this paper, the input voltage amplitude of the power grid is 311 V, the frequency is 50 Hz, and the phase difference is 120° three-phase alternating current. When a ground fault occurs in the power grid, a voltage drop will occur. When the fault is set at 0.6–1.4 s, the three phases A, B, and C of the grid voltage are all grounded, and the grid voltage returns to the normal value after 1.4 s. The fault is detected by the designed sliding mode observer. Since the three phases A, B, and C are all grounded, the voltage drop amplitude of each phase is the same, and the voltage drop is set as

$$u_g = U_g(1-h)e^{iw_g t}, \tag{20}$$

where U_g is the grid voltage amplitude, ω_g is the grid voltage electrical angular velocity, and h is the percentage of the fault degree. Figure 9 shows the tracing curve of the measured and observed values of the rotor current d-axis. Figure 10 shows the error curve between the measured value and the observed value of the rotor current d-axis. When the fault is added in 0.6 s, the sliding state is broken. The current value fluctuates greatly at first, and then quickly tends to 0 to reach a new balance. When the fault is removed at 1.4 s, the curve oscillates greatly, and convergence is reached again after 1.6s. It can be seen from the error curve that PSO-SMO has a smaller error, converges to 0 faster, and is more robust than traditional sliding mode observer. Figure 11 shows the tracking curve of measured and observed values of rotor current q-axis. Figure 12 shows the error curve between the measured value and the observed value of the rotor current q-axis. It has a similar change process with the d-axis current. By observing the residual value of the rotor current measurement value and the observation value, the fault detection of the system can be realized. At 0.6 s, the sliding mode is broken. The error value suddenly jumps to -0.15, and then gradually converges to 0, so it is judged that the system is malfunctioning at 0.6 s. The same is true for the q-axis. In ad-

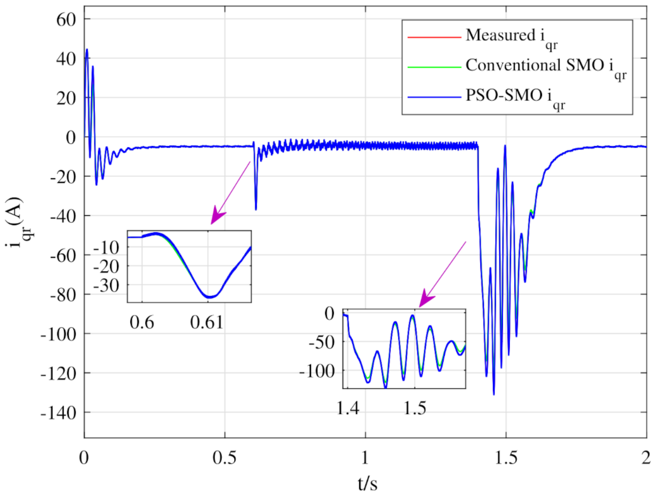

Fig. 11. Measured and observed tracking curve of rotor current q-axis

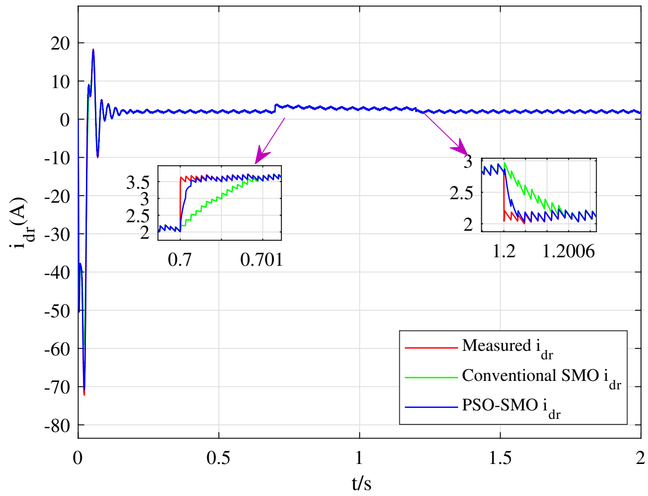

Fig. 13. Measured and observed tracking curve of rotor current d-axis

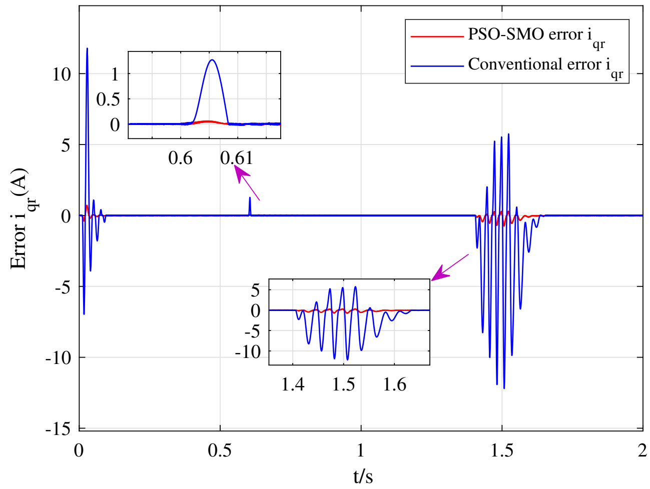

Fig. 12. Error curve between measured value and observed value of rotor current q-axis

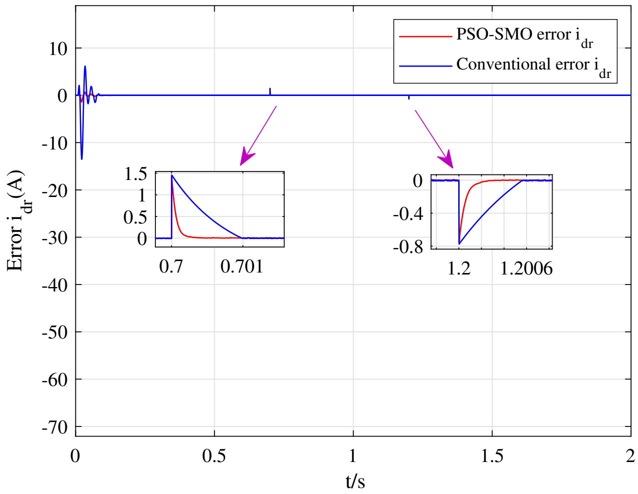

Fig. 14. Error curve between measured value and observed value of rotor current d-axis

dition, by comparing the PSO-SMO with the traditional sliding mode observer, it can be found that the traditional sliding mode observer has a great error when encountering a fault, while the PSO-SMO still has high stability.

5.4. Sensor failure

When the rotor current sensor fails, the rotor current sensor can be used for fault detection. Set the fault occurrence time to 0.7-1.2s, and the fault value is

$$d = \begin{cases} 0 & 0 \le t < 0.7 \\ 2e^{\cos(\pi t)} & 0.7 \le t < 1.2 \\ 0 & t \ge 1.2. \end{cases} \tag{21}$$

Figure 13 shows the tracing curve of the measured and observed values of the rotor current d-axis. Figure 14 shows the error curve between the measured value and the observed value of the rotor current d-axis. The result shows that the observation curve is basically consistent with the actual curve. When a fault is added at 0.7 s, a sudden change occurs in the curve, and then the error quickly approaches zero. When the sensor failure was removed at 1.2 s, the error curve showed small fluctuations, and then it quickly approached zero. Combining the observation curve and the error curve, it can be found that the sensor failure will break the sliding mode, and the normal sliding mode motion state cannot be restored during the failure period, so the sliding mode observer is very sensitive to the sensor failure. Figure 15 shows the tracking curve of measured and observed values of rotor current q-axis. Figure 16 shows the error curve between the measured value and the observed value of the rotor current q-axis. It has a similar change process with the d-axis current. In addition, comparing PSO-SMO with traditional sliding mode observers, it can be seen that the designed method has faster convergence speed and stability.

The three operating conditions of DFIG are analyzed above. This paper proposes the PSO-SMO method to observe the rotor current. Under normal operating conditions, the observation

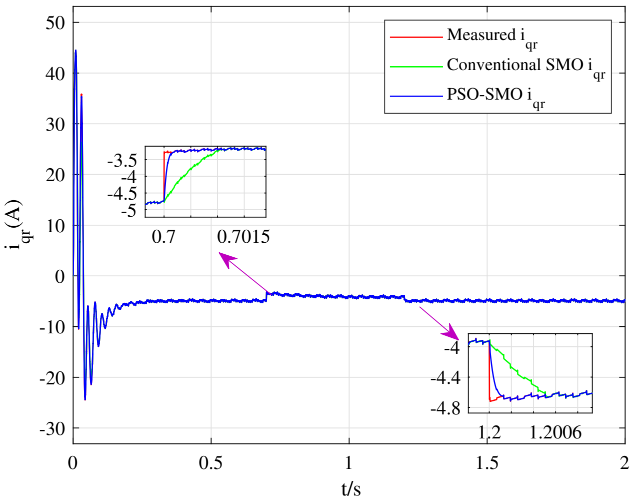

Fig. 15. Measured and observed tracking curve of rotor current q-axis

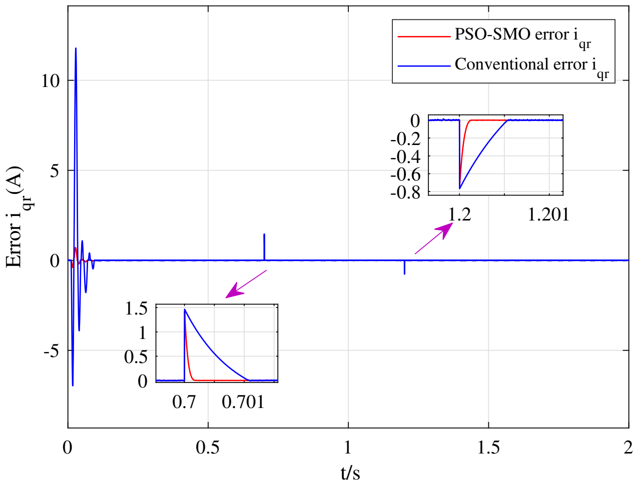

Fig. 16. Error curve between measured value and observed value of rotor current q-axis

error fluctuates around zero. When there is a large error between the measured value and the observed value, it indicates that the system may be malfunctioning. In summary, the PSO-SMO designed in this paper can observe the rotor current well. Compared with the traditional sliding mode observer, the response speed is faster, the accuracy is higher, and the chattering is smaller.

6. CONCLUSIONS

Due to improper selection of sliding mode parameters, the observation performance of the observer will be degraded, resulting in false alarms in fault detection. Therefore, for the problem that the parameters of the sliding mode observer are not easy to select, this paper uses the combination of the PSO algorithm and the sliding mode observer for fault detection of the DFIG. Compared with the traditional sliding mode observer, the proposed PSO-SMO method has better observation accuracy. In the event of failure, it has better stability and sensitivity. In addition, this paper sets up two types of faults, namely grid voltage drop fault and rotor current sensor fault. Through the designed sliding mode observer, three operating conditions are simulated and analyzed. The simulation results show that the designed sliding mode observer is sensitive to the failure of DFIG, and has the advantages of fast convergence speed, high accuracy and good stability.

REFERENCES

[1] H. Benbouhenni, N. Bizon, M.I. Mosaad, I. Colak, A.B. Djilali, and H. Gasmi, "Enhancement of the power quality of dfig-based dual-rotor wind turbine systems using fractional order fuzzy controller," *Expert Syst. Appl.*, vol. 238, p. 121695, 2024, doi: 10.1016/j.eswa.2023.121695.

[2] A.D. Bebars, A.A. Eladl, G.M. Abdulsalam, and E.A. Badran, "Internal electrical fault detection techniques in dfig-based wind turbines: A review," *Prot. Control Mod. Power Syst.*, vol. 7, no. 2, pp. 1–22, 2022, doi: 10.1186/s41601-022-00236-z.

[3] X. Jin, Z. Xu, and W. Qiao, "Condition monitoring of wind turbine generators using scada data analysis," *IEEE Trans. Sustainable Energy*, vol. 12, no. 1, pp. 202–210, 2021, doi: 10.1109/TSTE.2020.2989220.

[4] H. Habibi, I. Howard, and S. Simani, "Reliability improvement of wind turbine power generation using model-based fault detection and fault tolerant control: A review," *Renew. Energy*, vol. 135, pp. 877–896, 2019, doi: 10.1016/j.renene.2018.12.066.

[5] C. Xiao, Z. Liu, T. Zhang, and X. Zhang, "Deep learning method for fault detection of wind turbine converter," *Appl. Sciences*, vol. 11, no. 3, p. 1280, 2021, doi: 10.3390/app11031280.

[6] S. Ranjan Kabat, C. Kumar Panigrahi, and B. Prasad Ganthia, "Fuzzy logic based fault current prediction in double fed induction generator based wind turbine system," *Mater. Today-Proc.*, vol. 80, pp. 2530–2538, 2023, doi: 10.1016/j.matpr.2021.06.403.

[7] M. Kamarzarrin, M.H. Refan, and P. Amiri, "Open-circuit faults diagnosis and fault-tolerant control scheme based on sliding-mode observer for dfig back-to-back converters: Wind turbine applications," *Control Eng. Pract.*, vol. 126, p. 105235, 2022, doi: 10.1016/j.conengprac.2022.105235.

[8] Y. Zhang, T. Jiang, and J. Jiao, "Model-free predictive current control of a dfig using an ultra-local model for grid synchronization and power regulation," *IEEE Trans. Energy Convers.*, vol. 35, no. 4, pp. 2269–2280, 2020, doi: 10.1109/TEC.2020.3004567.

[9] M. Li, D. Yu, Z. Chen, K. Xiahou, T. Ji, and Q.H. Wu, "A data-driven residual-based method for fault diagnosis and isolation in wind turbines," *IEEE Trans. Sustainable Energy*, vol. 10, no. 2, pp. 895–904, 2019, doi: 10.1109/TSTE.2018.2853990.

[10] H. Wang, H. Wang, G. Jiang, Y. Wang, and S. Ren, "A multi-scale spatio-temporal convolutional deep belief network for sensor fault detection of wind turbine," *Sensors*, vol. 20, no. 12, p. 3580, 2020, doi: 10.3390/s20123580.

[11] W. Yu, Y. Lu, and J. Wang, "Application of small sample virtual expansion and spherical mapping model in wind turbine fault diagnosis," *Expert Syst. Appl.*, vol. 183, p. 115397, 2021, doi: 10.1016/j.eswa.2021.115397.

[12] E. Alizadeh, N. Meskin, and K. Khorasani, "A dendritic cell immune system inspired scheme for sensor fault detection and isolation of wind turbines," *IEEE Trans. Ind. Inf.*, vol. 14, no. 2, pp. 545–555, 2018, doi: 10.1109/TII.2017.2746761.

[13] A. Madhag and G. Zhu, "Online sensor ageing detection using a modified adaptive filter," *Int. J. Autom. Control*, vol. 14, no. 2, pp. 187–212, 2020, doi: 10.1504/IJAAC.2020.105518.

[14] H. Bastami, A.H. Abolmasoumi, and A.A. Ghadimi, "Stator voltage fault detection and optimal rotor current limiting in doubly fed induction generators," *Int. Trans. Electr. Energy Syst.*, vol. 27, no. 5, p. e2292, 2017.

[15] F. Shi and R. Patton, "An active fault tolerant control approach to an offshore wind turbine model," *Renew. Energy*, vol. 75, pp. 788–798, 2015, doi: 10.1016/j.renene.2014.10.061.

[16] M.-A. Yahiaoui, M. Kinnaert, and J. Gyselinck, "Augmented-state-observer-based diagnostics of open-circuit and sensor faults in dfig wind turbines," *IEEE Trans. Power Electron.*, vol. 38, no. 12, pp. 16 085–16 099, 2023, doi: 10.1109/TPEL.2023.3309737.

[17] M. Hou and H. Shi, "Stator-winding incipient shorted-turn fault detection for motor system in motorized spindle using modified interval observers," *IEEE Trans. Instrum. Meas.*, vol. 70, pp. 1–16, 2021, doi: 10.1109/TIM.2020.3040994.

[18] F. Marini and B. Walczak, "Particle swarm optimization (pso). a tutorial," *Chemom. Intell. Lab. Syst.*, vol. 149, pp. 153–165, 2015, doi: 10.1016/j.chemolab.2015.08.020.

[19] M. Jain, V. Saihjpal, N. Singh, and S.B. Singh, "An overview of variants and advancements of pso algorithm," *Appl. Sciences*, vol. 12, no. 17, p. 8392, 2022, doi: 10.3390/app12178392.

[20] R. Luo, Z. Wang, and Y. Sun, "Optimized luenberger observer-based pmsm sensorless control by pso," *Modell. Simul. Eng.*, vol. 2022, no. 1, p. 3328719, 2022.

[21] R. Li, W. Yu, J. Wang, Y. Lu, D. Jiang, G. Zhong, and Z. Zhou, "Fault detection for dfig based on sliding mode observer of new reaching law," *Bull. Pol. Acad. Sci. Tech. Sci.*, vol. 69, no. 3, p. e137389, 2021, doi: 10.24425/bpasts.2021.137389.

[22] L. Jia and X. Zhao, "An improved particle swarm optimization (pso) optimized integral separation pid and its application on central position control system," *IEEE Sens. J.*, vol. 19, no. 16, pp. 7064–7071, 2019, doi: 10.1109/JSEN.2019.2912849.

[23] S. Drid, M. Tadjine, and M.-S. Nait-Said, "Robust backstepping vector control for the doubly fed induction motor," *IET Control Theory Appl.*, vol. 1, no. 4, pp. 861–868, 2007.

[24] D.D. Reigosa, J.M. Guerrero, A.B. Diez, and F. Briz, "Rotor temperature estimation in doubly-fed induction machines using rotating high-frequency signal injection," *IEEE Trans. Ind. Appl.*, vol. 53, no. 4, pp. 3652–3662, 2017, doi: 10.1109/TIA.2017.2684742.